



**HAL**  
open science

## **Flax xylem as composite material reinforcement: Microstructure and mechanical properties**

Lucile Nuez, Anthony Magueresse, Pin Lu, Arnaud Day, Thomas Boursat,  
Pierre d'Arras, Patrick Perré, Alain Bourmaud, Christophe Baley

### ► To cite this version:

Lucile Nuez, Anthony Magueresse, Pin Lu, Arnaud Day, Thomas Boursat, et al.. Flax xylem as composite material reinforcement: Microstructure and mechanical properties. *Composites Part A: Applied Science and Manufacturing*, 2021, 149, pp.106550. 10.1016/j.compositesa.2021.106550 . hal-03487074

**HAL Id: hal-03487074**

**<https://hal.science/hal-03487074v1>**

Submitted on 2 Aug 2023

**HAL** is a multi-disciplinary open access archive for the deposit and dissemination of scientific research documents, whether they are published or not. The documents may come from teaching and research institutions in France or abroad, or from public or private research centers.

L'archive ouverte pluridisciplinaire **HAL**, est destinée au dépôt et à la diffusion de documents scientifiques de niveau recherche, publiés ou non, émanant des établissements d'enseignement et de recherche français ou étrangers, des laboratoires publics ou privés.



Distributed under a Creative Commons Attribution - NonCommercial 4.0 International License

## Flax xylem as composite material reinforcement: Microstructure and mechanical properties

Lucile Nuez <sup>a, b</sup> ; Anthony Magueresse <sup>a</sup> ; Pin Lu <sup>c</sup> ; Arnaud Day <sup>d, e</sup> ; Thomas Boursat <sup>a</sup> ; Pierre D'Arras <sup>b</sup> ;  
Patrick Perré <sup>c</sup> ; Alain Bourmaud <sup>a</sup> ; Christophe Baley <sup>a</sup>

a : Université de Bretagne-Sud, IRDL, CNRS UMR 6027, BP 92116, 56321 Lorient Cedex, France

b: Van Robaeys Frères, 83 Rue Saint-Michel, 59122 Killeem, France

c: Université Paris-Saclay, CentraleSupélec, Laboratoire de Génie des Procédés et Matériaux, SFR  
Condorcet FR CNRS 3417, Centre Européen de Biotechnologie et de Bioéconomie (CEBB), 3 rue des  
Rouges Terres, 51110 Pomacle, France

d: CNRS, UMR8576, UGSF- Unité de Glycobiologie Structurale et Fonctionnelle, Unité de Lille, 59000  
Lille, France

e: Fibres Recherche Développement, Technopole de l'Aube en Champagne – Hôtel de Bureaux 2, 2 rue  
Gustave Eiffel, CS 90601, 10901 TROYES, Cedex 9, France

\* Corresponding author: *e-mail address* lucile.nuez@univ-ubs.fr

Tel.: +33-2-97-87-45-08; Fax: +33-2-97-87-45-18

### Abstract

Flax shives have been proven to be relevant injection-moulded reinforcement materials with a stiffness that reaches 90% of that obtained with cut flax fibres. Nevertheless, little is known of the reinforcing mechanisms of this material. In this study, deeper insight is sought on the mechanical properties of flax shives, which originate mainly from the xylem tissue of the flax stems. The microstructure of flax xylem is investigated by nanotomography and image analysis as a function of stem height, combined with AFM measurements of the cell walls in Peak Force Quantitative Nano Mechanical indentation mode (20-22 GPa were measured for the S2 layer). The bending stiffness of peeled flax stems was furthermore investigated, and finally, an estimation of the flax shive particle stiffness was carried out and tested with a micromechanical approach in order to evaluate their reinforcing potential in injection-moulded composites.

**Keywords:** A. Natural Fibres; B. Microstructures; A. Biocomposite; B. Mechanical properties

## 1. Introduction

The current environmental changes present a substantial motivation for the development of eco-responsible materials for technical applications, such as bio-based composites or bio-inspired materials and structures. One of the leading plants for composite reinforcement in Europe is flax, due to its wide availability and its outstanding properties. Flax (*Linum usitatissimum L.*) is an angiosperm dicotyledon plant of the linaceae family. For composite applications, flax is commonly cultivated annually for its bast fibres that exhibit significant specific mechanical properties, comparable to those of glass fibres [1].

However, flax shives, the greatest by-product obtained from the scutching process, represent up to 50% of the biomass weight after retting [2]. With over 124,000 ha of flax cultivation areas in 2018 over France, Belgium, and the Netherlands, flax shives represent roughly 400,000 tons of available biomass for these three countries alone. They are used mainly as animal bedding or agglomerated panels [3], but they have also been examined as a resource for various innovative applications including activated carbon [4], 3D-printed lightweight concrete [5], bio-fuel production [6], or as a substitute for wood flour in extruded wood-plastic composites [7] [8]. Investigations of the reinforcing **capacity** of flax shives as polymer reinforcement material have proven their potential [9]; nevertheless, a greater knowledge of the mechanical performance of flax shives is needed in order to fully appreciate their role in the reinforcement of biocomposites.

Flax shives come from the scutching industrial transformation of the retted flax straw. Through the action of fluted rollers and rotating steel turbines, the straws are crushed, then beaten to separate the inner tissues of the plant, the shives, from the high added-value fibres. **They** are viewed as a cause of quality defects in the subsequent fibre transformation processes. Flax shives are made up of approximately 20-30% lignin, 30-50% cellulose, and 20-25% hemicelluloses depending on the measurement methods, plant maturity, and location in the stem [10][11]. Day et al. [12] found that lignin content increases from approximately 24% to 31% for the basal part of the stem inner tissues between the stages of flowering and of seed maturity. This is remarkably higher than the lignin content of flax bast fibres, which lies in the range of 2-5% depending on the maturity stage of the plant [13], therefore potentially impacting the fibre-matrix adherence quality [14].

Also called woody core, flax shives originate from the plant's inner tissues, and most importantly from its xylem, whereas the flax fibres commonly used for textile reinforcement of composite applications come from the supporting phloem tissue. However, whereas the mechanical properties of flax bast fibres have been extensively investigated [15][16], those of the flax xylem are not very well known.

Due to the hollow nature of the cells, their short length, and the cohesion between xylem cells, extraction and tensile experiments are difficult to implement on individual cells even though some specific tests have been developed by the wood research community [16] [17]; the main bottleneck in this case is the handling of fibres and the accurate determination of specimen strain during the tensile tests. However, the wood and plant fibre research community has developed suitable methods, using nanoindentation or atomic force microscopy (AFM), to locally investigate the mechanical behaviour of plant fibre cell walls. The main differences between the two methods are the tip geometry (sharper in case of AFM) and the penetration depth (80-120 nm and 2-3 nm for nanoindentation and AFM, respectively), which induce a higher impact of sample roughness, environmental conditions, and adhesion forces if AFM is chosen [19], [20]. However, the relevance of Atomic Force Microscopy in Peak Force Quantitative Nano Mapping (AFM-PFQNM) measurements has been demonstrated when compared with nanoindentation [21]. Even though both methods have been shown to be well-suited to comparative measurements, AFM-PFQNM, owing to its high resolution, is better adapted to highlight changes in interlayer stiffness at the local scale [20], especially if thin layers are considered.

The mechanical characterization of flax stems is difficult due to their complex and anisotropic structure involving narrow cell walls. Although the rigorous 4-point bending test can be applied to minute samples [22], the 3-point bending test is a convenient and accessible method due to the required simple machine apparatus and setup, and it is applicable to stems, with a few caveats. Several factors may lead to an underestimation of strength and elastic modulus, such as stress concentration at the loading point or supplementary induced shear stresses during bending [23]. Nevertheless, the xylem has a significant role in the mechanical support of the stem, and it was measured to account for up to 30% of a dry flax stem bending stiffness [24].

This study focuses on **a multi-scale investigation of** the xylem of flax to gain further insight into its microstructure and greater understanding of the reinforcing mechanisms when flax shives are used as injection-moulded composites reinforcement. This could lead to the development of a new field of

application for this widely available resource, in accordance with the necessary environment-friendly industrial transformation. First, a fine description and microstructural analysis of the xylem is given with the support of both nanotomography and scanning electron microscopy (SEM) observations of the flax stem. This is followed by a study **at the cell wall scale** of the mechanical properties of the xylem by atomic force microscopy (AFM) in peak force quantitative mapping and indentation modulus analysis mode, and **at the flax stem scale** by 3-point bending tests. Finally, the mechanical properties of flax shives in injection-moulded composites are **estimated and** investigated through a micromechanical approach.

## 2. Materials and Methods

### 2.1. Materials

#### 2.1.1. Flax stems

Aramis variety flax stems were provided by Van Robaeys Frères (France), grown in the Somme region (France) in 2018 with a seeding rate of 1750 seeds/m<sup>2</sup>. **They were** pulled-out at fibre maturity, which corresponds to the general pull-out stage of flax, in this case 120 days after sowing. They were air-dried and did not undergo any retting. Samples were collected along the technical length of the stem, defined as the length from above the cotyledon to the first seed capsule ramifications [25][26]. This technical length was divided into three equal sections; each section was then cut symmetrically from both sides to obtain 20 cm long segments named C1, C2, and C3 for the lower, middle, and upper sections respectively, as shown in Figure 1a. From those segments, the sclerenchyma (bast) fibres and surrounding tissues, apparent at the periphery of the cross-section SEM image of the flax stem shown in Figure 1b, were **thoroughly** removed, first manually then by very carefully scraping a 2,400-grain glass paper around the stem in order to keep the xylem intact. Two more points were further examined: C0 and C4 at the base and top of the technical length respectively, C4 being approximately 10 cm above C3, and C0 approximately 10 cm under C1. These samples were examined by 3-point bending tests and by image analysis following vibratome slicing, described in section 2.2.4.

AFM investigations were carried out on a flax xylem sample from the Eden variety, provided by Terre de Lin (France) and grown in 2016 with a conventional seeding rate of 1,800 seeds/m<sup>2</sup>. The sample was pulled out after 120 days and a cumulative growing degree-day (GDD) of 1,076 °C, which corresponds to the fibre maturity growth stage.

### 2.1.2. Flax shives

Flax shives were used as injection-moulded composite reinforcement material. Originating from the scutching of flax harvested in 2018, they were provided in bulk by the flax scutching company Van Robaey Frères (France). The flax shives were milled with a laboratory scale rotating cutting mill (Retsch Mühle, Germany) with a 500 µm mesh size grid, and they were then oven-dried at 80°C overnight and further fractionated using a vibrating sieving column. Only the fraction of particles between the 400 and 630 µm mesh sized sieves was recovered and used as composite reinforcement as it visually constituted a cellular structure representative of the xylem because it preserves the cellular structure of the xylem after fragmentation (Figure 2). The flax shives (FS) were oven dried at 80°C for at least 12h before further processing.

### 2.1.3. Injection moulding polymer matrix

For injected composite manufacturing, the matrix used was poly(propylene) PPC 10642 (Total Petrochemicals, France) with a Melt Flow Index (MFI) of 44 g/10 min at 230°C and 2.16 kg and with a density of 0.94. To this, maleic anhydride modified poly(propylene) (MAPP) Orevac CA 100 was added (Arkema, France), with an MFI of 10 g/10 min at 190°C and 0.325 kg. MAPP acts as a compatibilizer due to its amphiphilic nature and 4%-wt were chosen to be added to the formulation as previous studies have shown it represents a good compromise between bonding improvement and the polymer cost [27].

## 2.2. Methods

### 2.2.1. Nanotomography

A flax stem was scanned at a voxel size of (500 nm)<sup>3</sup> with a nanotomograph EasyTom XL 150/160 manufactured by RX-solutions (Annecy, France). A nano-focus vacuum tube with a LaB6 filament for X-ray emission at a working voltage of 100 kV and working current of 175 µA was used. A CCD detector of 2004 × 1336 pixels was selected and a total of 1568 radiographs were obtained, each with an exposure time of 2 seconds and an average of five frames. The image reconstruction was performed with XAct<sup>®</sup>. By building up the stack of 2D images obtained from reconstruction, the 3D volume of the sample was achieved using Avizo 2019.2 (Thermo Scientific<sup>™</sup>).

### 2.2.2. Atomic Force Microscopy (AFM)

The measurement of the indentation modulus of flax xylem was conducted by atomic force microscopy (AFM) in Peak Force Quantitative Nano Mechanical (PF-QNM) mode. One cm long samples were cut from the middle of the Eden stems immediately after plant pull out at fibre maturity. The embedding protocol is fully described in Goudenhoofdt et al. [28]; samples were then cut using an ultramicrotome (Leica Ultracut R) equipped with diamond knives.

A multimode AFM instrument (Bruker Corporation, USA) with a peak-force quantitative nanomechanical mapping imaging mode was used to measure the nanoindentation modulus of xylem cells. A RTESPA-525 (Bruker, USA) probe with a spring constant of 139 N/m, a tip radius between 15 and 35 nm, a scan rate of 8  $\mu\text{m/s}$ , and a maximum load of 200 nN were used in the measurements. The calibration of the tip and cantilever of the probe are described in Arnould et al. [20]. To control the AFM measurements, both the embedding resin and some locations in the cell wall S2-G layer of the xylem sample were measured for the nanoindentation modulus.

### 2.2.3. Three-point bending tests

Three-point bending tests were carried out on each stem section (C1, C2, and C3 as shown in Figure 1a) in controlled environmental conditions (temperature of  $23 \pm 1$  °C and relative humidity of  $48 \pm 2\%$ ) on a universal MTS tensile machine with a 50 N capacity load cell in 10 repetitions. To avoid sample cross-section ovalization, which would change the actual sample cross-section and therefore affect its elastic modulus, a rounded loading anvil with a radius of 0.5 mm was chosen. Shear stresses can be minimized with respect to normal stresses by choosing a span-to-diameter ratio (where the span is the distance between the supports and the diameter refers to that of the sample) sufficiently high so as to limit shear stresses and prevent cross-section deformation, which also depends on the hollowness ratio of the stem [23]. In order to neglect these phenomena, a support span length of 180 mm was chosen, based upon previous studies, which represents a span-to-depth ratio of at least 80 for flax [24].

The displacement rate was fixed at 0.1 mm/s until the sample longitudinal strain at the external faces of the stem reached 5% in order to preserve the elastic behaviour of the stems. The stem diameter was assessed by optical measurements of the stem cross-section after carefully cutting the stem and taking

care not to flatten the section. The xylem apparent stiffness was obtained by considering the stem as a uniform beam with a circular cross-section. As the effects of shear strain, section ovalization, and compressive strain at loading points can be neglected, the displacement  $y$  in the middle of the section can then be given by Equation 1:

$$y = \frac{4}{3} * \frac{F * L^3}{\pi D^4 * E} \quad \text{Eq. 1}$$

With  $F$  the force applied to the sample,  $L$  the span length,  $D$  the stem diameter and  $E$  the bending modulus. In this simple approach, the apparent stiffness is calculated assuming the sample is assimilated to a cylinder of diameter  $D$  equal to that of the xylem tissue.

#### 2.2.4. Image analysis of the xylem microstructure

Analysis of the internal structure of the xylem was carried out by image analysis from the cross-sections of the xylem at C1, C2, and C3, in the middle of each stem segment (Figure 1a). In order to achieve high quality images, stems were embedded in a 5%-wt aqueous solution of agarose (Euromedex, France), and were left to harden overnight. The cross-sections were obtained by cutting slices of a thickness between 50 and 150  $\mu\text{m}$  using a Leica VT1000 S vibratome. The slicing was carried out with a thin metal blade at a cutting speed of 0.05 mm/s and a frequency of 60 Hz.

The cross-sections obtained were further sputter-coated with a thin layer of gold in an Edwards Sputter Coater. Images were manually edited in order to analyse precisely the surface of the cells. The ImageJ® software was used to measure cell-wall thickness as well as cell morphology and area as function of the centre of the stem. Matlab software was also used to analyse cell size as a function of the normalised position of the cells in the xylem tissue,  $d$ , given by Equation 2:

$$d = \frac{r_x - r_i}{r_e - r_i} \quad \text{Eq. 2}$$

With  $r_x$  the centre of the cell,  $r_i$  and  $r_e$  the inner radius and exterior radius of the xylem tissue respectively.

#### 2.2.5. Composite manufacturing

Before processing, the reinforcing flax shives and the PP-MAPP matrix were oven dried at 60°C for at least 12 hours. They were then compounded with a co-rotating twin-screw extruder TSA (Italy) with a screw diameter of 20 mm and L/D ratio of 40. A temperature profile going from 180°C to 190°C and a

die temperature of 180°C were imposed with a screw rotation speed of 300 rpm. The material was then granulated, oven-dried, and ISO 527-2 type 1B normalized specimens were obtained using an 80 Tons Battenfeld (Austria) injection moulding machine with a constant barrel and mould temperature set at 190°C and 30°C, respectively.

#### 2.2.6. Mechanical characterization

The injection-moulded T-bone specimens were submitted to tensile testing following the ISO 527 standard on an MTS Synergie 1000RT machine with a controlled environment (temperature of 23°C and relative humidity of 48%). The tensile speed was 1 mm/min and the nominal gauge length was 25 mm. A 10 kN sensor was used to measure the force applied on the specimen, and an extensometer was used to measure deformation during the tests.

### 3. Results

#### 3.1. Study of the xylem microstructure

##### 3.1.1. Fine description of the xylem

X-ray nanotomography offers an accurate overview of the cellular organization of the flax stem without any artefacts due to surface preparation (Figure 3a). In this section, corresponding to an apical part of the stem, the different tissues can be easily distinguished as the secondary development due to the cambial activities is weaker than in the basal part of this organ. Figure 3a presents both the 3D computer reconstitution of the stem tissue organization and its cross-section slice in 2D corresponding to a transverse stem section as illustrated in Figure 3b-e issued from SEM photographs.

The outer tissues, including epidermis, cortical parenchyma, bast fibres (from which the lumens are not visible at this resolution), secondary phloem, and vascular cambium, are composed of cells walls with low lignin content compared to the xylem tissues (Figure 3a). The latter form the major part of the internal tissues and exhibit near 10-fold more lignin in their cell walls compared to the outer tissues [12]. As the resolution of X-ray tomography is close to the X-ray absorbance of the cell wall, the link with the lignin content could be suggested. Popescu et al. [29] have reported an influence of X-ray diffraction pattern and lignin content in softwood and hardwood.

The cellular organization of these internal tissues shows two patterns (Figure 3a, b). In the area close to the vascular cambium, cells with a thick cell wall appear aligned, whereas a more disorganized pattern takes place in the centre of the stem. This difference betrays their cellular origin since flax growth arises from mitotic cell divisions taking place in two types of meristem. The primary meristems contribute to the plant elongation whereas secondary meristems, formed after the tissues of the primary plant body have differentiated, are responsible for the girth increase. Contrary to the former, secondary meristems, named cambium, contain initial cells that divide by periclinal divisions (parallel to the surface of the axis) on their inner and outer faces, producing files of cells along the radii of the axis [30]. Relevant to the vascular cambium, the most active secondary meristem in flax, new cells pass into the secondary xylem and phloem domains, respectively [31]. In the centre of the stem, two primary tissues are distinguished. At the periphery of the pith characterized by cells having an important size and a thin cell wall, some bulk of primary xylem is noticeable. It is disposed on one circle and contains cells with different diameters with a thicker cell wall (Figure 3a-c).

Through their usual name, flax shives correspond to these internal tissues and so include a large diversity of cells. Considering the thin cell wall of pith cells that are crushed with scutching of flax stem, the flax shives used in the industry correspond to the xylem tissue of flax stems. The xylem plays a double function in vascular plants: as water and nutrients transport from roots to leaves and as mechanical support for the upright posture of the stem. The primary xylem is formed in the stem by the primary meristem in the apical part of the stem. Then, a secondary growth takes place, involving the differentiation of the vascular cambium at the periphery of the primary xylem. The development of this vascular cambium conducts to the secondary xylem [30][32]. Both primary and secondary xylems are formed with cells of different sizes and distinctive cell walls closely linked with plant development and tissue functions. The flax stem primary xylem (Figure 3b, c) shows two characteristic elements: tracheid and vessel elements, characterized by their typical secondary wall thickening. As noticeable in Figure 3a, tracheid elements are spindle shaped, elongated, and have tapering ends, whereas vessel elements have perforated end walls forming a tube-like structure facilitating water conduction. Vessels differentiated after tracheids to follow young stem development. Both cell types present various but typical secondary wall patterns on their side walls, including rings (annular tracheid), helical (helical tracheid) and scalariform (scalariform vessel) (Figure 3d, e).

The flax secondary xylem appears mainly composed of two types of cells with different diameters (Figure 3b). Figure 3a, presenting both transversal and longitudinal views of the flax stem section, shows the presence of cells with tapered end, a typical characteristic of tracheids. The cell walls of larger cells present numerous perforations (Figure 3b, c) contrary to cells of smaller diameter. These perforations, named pits, correspond to an area where only the primary wall and middle lamella are present. Except at these perforations, the primary wall is covered by the secondary wall, which suggests that these elements are not extensible and have matured after the axis has ceased its elongation growth. From this observation, it could be suggested that large diameter cells could be fibre tracheid cells playing both water transport and mechanical support functions. Therefore, small diameter cells could be xylem parenchyma cells with a lateral transport function. These results and hypothesis are consistent with previous observations on other flax cultivars grown under different agronomic conditions [33][34][12]. In addition, Lion et al. [33] drew attention to the different profiles of cell wall lignification between these two types of cells related to their different biological roles. However, this organization contrasts with the classical view of the eudicotyledon secondary xylem such as Arabidopsis [32], hemp [35], poplar [36], or ring-porous wood species [37] in which large water-conducting vessels are present with fibre cells acting as support function and parenchyma playing the role of lateral transport. Secondary xylem organization and composition are well known to depict a high variability across different plant groups [30]. The length of these fibre tracheid elements in the present study varies in a range of 150 to 200  $\mu\text{m}$ , conflicting with the typical length of fibre tracheids found in other species: 1.18 to 7.39 mm in conifers or 0.77 to 2.3 mm for fibres found in Angiosperms [38]. However, Carlquist et Schneider suggest to be **cautious** on unequivocal classifications and the presence of varied exceptions [39]. Moreover, vesselless woods, as suggested by these observations, have been reported as an advantage in water provision through their greater cavitation resistance and therefore better tolerance of stressful conditions [40].

### 3.1.2. Microstructure as a function of stem height

After removing external tissues (from epidermis to vascular cambium), the microstructure evolution of the xylem as a function of stem height was examined from transversal views of the xylem. In the SEM images of each stem section, shown in Figure 4, the xylem tissue is intact and no fibre bundles or individual fibres are present around it, which validates the method of bast fibre removal.

Figure 4 shows the evolution of global morphology of the xylem with stem height. Results show a clear decrease in xylem tissue surface with increasing stem height, with an 82% drop between C0 at the base of the stem to C4 at the top. In 1942, Tiver also measured an 80% drop in xylem surface from the base of the stem at the cotyledon to the first ramifications [41]. While the varieties and cultivation practices have evolved since then, the overall flax xylem architecture remains similar.

The thickness of the xylem tissue, taken as the difference between the external and the inner radius, evolves similarly, with an initial thickness of  $604 \pm 21 \mu\text{m}$  for C0 that quickly drops to  $380 \pm 20 \mu\text{m}$  at C1, and decreases to  $193 \pm 21 \mu\text{m}$  for C3. Figure 4 also shows a pith surface that first increases from the base of the stem at C0 to C1 from approximately  $0.31 \text{ mm}^2$  to  $0.90 \text{ mm}^2$  respectively, then slowly decreases until C4 at  $0.30 \text{ mm}^2$ , as has also been observed by Tiver [41].

Figure 5a-c gives an example of the cell surface distribution within a portion of the cross-section of C1, C2, and C3 samples respectively. It is possible to see, in dark red, cells with areas greater than  $700 \mu\text{m}^2$  towards the centre of the stem. These cells correspond to the pith of the stem. They are surrounded by a large number of cells with an area inferior to  $100 \mu\text{m}^2$  forming primary xylem tissue poles as described previously (Figure 3). When considering the cells departing from the primary xylem poles and situated towards the outer radius of the stem cross-section, in the secondary xylem, it appears that their surface is relatively homogeneous in comparison with the xylem tissue of other angiosperms such as hemp or poplar [35][36]. An important number of cell areas between  $300$  and  $400 \mu\text{m}^2$  and some smaller cells of less than  $200 \mu\text{m}^2$  are visible, corresponding to both fibre tracheids and ray parenchyma as seen more precisely in Figure 3b and c.

In Figure 5d-f, it is possible to visualise the mean cell surface distribution as a function of the normalised position of the cells **across the width** on the xylem tissue and **for different** stem height (see section 2.1.1 for reference to sample location in the stem) for a representative  $1/6^{\text{th}}$  of the xylem tissue cross-section. The largest cells are visible at the centre of the stem and come from the pith, as seen in dark red in Figure 5a-c. This is visible for all stem heights, followed by a sharp decrease in cell surface at 0.2 of the normalized position across the width of the xylem tissue as cells become either the tracheid or vessel elements that characterize the xylem tissue. A sharp decrease in cell surface is then visible until approximately 0.3 of the normalized position across the xylem tissue, because of the presence of the primary xylem, illustrated for C1 (the bottom stem section) in Figure 4.

Regardless of stem height, the xylem cell surface of all samples comes to a plateau from approximately 0.35 of the normalized position in the xylem tissue, at 416, 147, 104  $\mu\text{m}^2$  for C1, C2, and C3 respectively. The cell surface then decreases slowly for C1, C2, and C3 until 0.9 of the normalized position in the xylem tissue, which corresponds to the decrease of the cell surface as the cells get closer to the stem's vascular cambium. The xylem tissue thickness is much lower for C3 compared to C1 and C2, and the amount of the secondary xylem is low compared to the rest of the stem. Furthermore, slight crushing of the cells at the border of samples during their preparation may further diminish the cell surface at the edge of samples.

Figure 6a-c illustrates the cell wall thickness distribution throughout a portion of the xylem tissue for the three stem heights investigated, C1, C2, and C3 respectively. Each image clearly shows a gradient in thickness as a function of distance from the centre of the stem, with thickening of the cell wall from approximately less than 2  $\mu\text{m}$  to over 4  $\mu\text{m}$  as the distance from the centre of the stem increases. In Figure 6a and b, the few areas where the thickness of cell walls exceeds 8  $\mu\text{m}$  are due to artefacts in the SEM image because of crackling caused by the vibratome cut of the section.

The gradient in cell wall thickness follows the developing stage of the stem, with thicker secondary xylem cell walls and thinner primary cell walls (less than 2  $\mu\text{m}$ ). The proportion of the primary xylem decreases as the height of the stem increases. In the case of bast fibres such as flax or hemp, fibres at the base of the stem achieve maturity with a more important lignification given that their mechanical role is important [16][42][43].

### 3.2. Study of the xylem mechanical properties

#### 3.2.1. AFM-PFQNM analysis of the xylem cells

The nano-mechanical properties of the secondary xylem cell were analysed at fibre maturity stage, which corresponds to the general pull-out stage of flax (in this study, 120 days after sowing), by atomic force microscopy in peak-force quantitative nano-mechanical mapping mode. The AFM image of the xylem cell walls at mid-stem in Figure 7a shows different cell wall layers that display a gradient in mechanical properties. Figure 7b is a detailed view of the Figure 7a and highlights the main layers of the cell wall overall architecture; it is visible that the general organization is similar to that of bast fibres with

successive middle lamella (ML) and then primary and secondary S1, S2, and S3 layers. The main difference with peripheral fibres is the thin wall thickness S2, which is only about 2-3 microns. The measured modulus of indentation is given in Figure 7c as a function of the cutting line shown in Figure 7a and Figure 7b. The middle lamella is observed to have the lowest indentation modulus, at approximately 12 GPa (Figure 7c). This value is well correlated with the literature data where values between 10 and 12.5 GPa are reported for the ML of mature flax bast fibres [44], [45]. It is also possible to estimate the stiffness of the S2 and S3 layers, as their indentation moduli are about 20-22 and 16 GPa. In this study, the order of magnitude of the xylem cell wall indentation modulus is slightly higher than the values obtained by Goudenhooff et al. [28] for flax bast fibres at the same stage of growth, always by AFM-PFQNM. However, these measurements should be compared with caution, as the biochemical composition of xylem and bast fibres cell walls is significantly different, **bast fibre secondary cell walls being of gelatinous type while flax xylem secondary cell walls are of xylan type** [46].

Jäger et al. [47] have modelled the value of the wood indentation modulus as a function of cell wall structural parameters. It appears that the indentation modulus is positively correlated with the wall cellulose content and inversely with the MFA; however, we do not have reliable values of the MFA of the S2 layer of these cells. The high values measured in AFM-PFQNM suggest that it is probably relatively low. However, it should be kept in mind that the biochemical assays mentioned were performed on a mixture of shives cells, not necessarily representative of the cell explored in Figure 7.

### 3.2.2. Flexural properties of the xylem tissue

At a macroscopic scale, 3-point bending tests were carried out on flax stems from which the fibre bundles were peeled off so as to examine the xylem only. **The aim of this is to investigate the mechanical properties of the xylem depending on the sampling zone along the stem.** Results of the apparent modulus (**apparent car depend microstructure et propriétés des parois**) are given in Table 1 for different stem heights. The apparent bending modulus of C1 is comparable to that of C2, at  $6,223 \pm 710$  MPa and  $6,160 \pm 597$  MPa for C1 and C2 respectively. The mean stiffness of the flax xylem was measured by the same 3-point bending method to be  $6,200 \pm 1,800$  MPa by Réquillé et al. [24] for samples originating from the middle of the stem, which corresponds to a relative difference of 3% and validates our method.

Regarding the top section of the stem (C3), the bending stiffness is  $7,124 \pm 781$  MPa, approximately 14% and 16% higher than that of C1 and C2 respectively. A one-way **analysis of variance** (ANOVA) **statistical** test carried out **for these three groups** validates this statistical difference. The F-value is 5.44, showing the null hypothesis is rejected, which means that at the 0.05 level, the population means are different. A Fisher test for all samples concluded there was no significant difference between the bottom (C1) and the middle (C2) sampling locations, but there was a significant difference of C3 with respect to C1 and C2. One of the two main functions of the xylem cell tissue is to provide mechanical support to the stem, in particular in order to maximize its lodging resistance, which depends directly on the bending stiffness and height of the stem. This is done in combination with the sclerenchyma (bast) fibres, measured to be accountable for 65-75% on the bending stiffness of dry flax stems [24]. In order to maximise the bending stiffness of a beam structure, the tissues of highest stiffness should be positioned at its periphery. This is the case for the flax stem, and this important structural effect should be taken into consideration [48]. These results were obtained considering each xylem stem portion to be a full cylindrical beam. This is undoubtedly an important approximation as the samples examined are far from perfect cylindrical sections (as seen in section 3.1), and the stem is rather conical when considered from bottom to top. In addition, the cell structure variation through each xylem stem section could explain the differences in apparent bending modulus of C3 against C1 and C2. Moreover, there are many factors that cannot be considered directly at the stem scale. Different cell maturity stages throughout the stem height, variation in cellulose MFA, gradient in biochemical composition distribution, and varying secondary xylem organization are all elements of the highly anisotropic behaviour of cell walls, which makes it difficult to measure specific cell wall stiffness. Various studies have nevertheless focused on the mechanical modelling of the structure-mechanical relationship of plant cell walls within a cell tissue by finite element analysis [49][50]. As the apparent bending modulus is in the same order of magnitude, the flax xylem will further be examined as reinforcement material in injection-moulded composites.

### **3.3. Reinforcing mechanisms of the xylem in injection-moulded composites**

Flax shives originate mainly from the xylem tissue following scutching, the first industrial transformation step of flax. In industrial shives, however, other parts of the stem can be found in flax shives, such as

parts of stem roots or seed capsule residues. In order to specifically evaluate the role of the xylem tissue in the reinforcement of poly-(propylene) injection-moulded composites, the knife-milled flax shives were further sieved so that only the fraction of particles between the 400 and 630  $\mu\text{m}$  sized meshes were used. Their mechanical properties were further compared with those obtained by unsieved fragmented flax shives of a previous study [9] and are given in Table 2. No significant difference in the composite mechanical properties are observed, despite a greater aspect ratio for the sieved flax shives and a smaller particle size distribution.

The following paragraph aims at giving an estimation of the mechanical properties of flax shives in the form of particulate reinforcement of injection moulded composites, which will then further be tested through the help of a micromechanical model. It is first necessary to know the elastic properties of the reinforcing flax shives. The indentation modulus measured previously (section 3.2.1) gives information at a very local scale by means of AFM analysis but cannot be directly linked to of the tensile stiffness of the flax shives [20]. Moreover, the apparent stiffness measured by the 3-point bending test of the xylem (flax stems after removal of the fibres, see section 3.2.2) cannot straightforwardly be used in this estimation because of the heterogenous microstructure of the xylem with varying cell wall thicknesses and cell surface. The bending solicitation is in reality complex and does not directly give access to the elastic properties of flax shives as they are in the form of particles. Furthermore, inside the polymer matrix of the injection moulded composites the latter are solicited by longitudinal and transversal tensile and shear stresses.

The biochemical composition of flax shives is very close to that of hardwood, with a cellulose, hemicellulose, and lignin content of 46, 22, and 25% respectively, in particular in the type of hemicelluloses present in flax shives, with an important amount of xylan [9][11][51]. The xylem cells also have a multi-layered structure comparable to that of wood, as shown in section 3.2.1, with a well-visible middle lamella and the primary and secondary cell walls, the latter being made up of the S1, S2, and S3 layers as well as a large-size lumen, oppositely to bast flax fibres. Furthermore, many authors have shown the correlation between wood density, its elastic properties, and the elastic properties of its cell walls [52][53]. The density of the injection moulded composites was measured by weighing in ethanol and air for several FS weight fractions (from 0 to 40%) [54][55]. By considering a composite with a FS mass fraction of 100 %, the linear regression ( $R^2 = 0.9952$ ) was used to give a density of 1.237  $\text{g/cm}^3$

for the flax shives particles as they are in the composite. This surprisingly important density is explained by the fragmentation of part of the cells during processing and the creation of fines, leading to an estimated density closer to that of the cell wall than of the bulk and porous material [9].

Knowing the density of flax shives in the composite, and knowing the linear relationship between wood density and its elastic properties [52][53], the elastic properties of flax shives were estimated using the empirical equations given by [53]. The results are presented in Table 3.

These estimations were tested at the scale of the composite using a micromechanical model, which must account for (i) highly isotropic reinforcing material properties, (ii) its orientation, (iii) its aspect ratio, and (iv) its volume fraction. The longitudinal modulus  $E_L$  and transverse modulus  $E_T$  for a ply reinforced by short unidirectional fibres are estimated by Equations 3 and 4 as proposed by the Halpin-Tsai model [56]:

$$\frac{M}{M_m} = \frac{1+\xi*\eta*V_f}{1-\eta*V_f} \quad Eq. 3$$

$$\eta = \frac{\frac{M_f-1}{M_m}}{\frac{M_f}{M_m}+\xi} \quad Eq. 4$$

Where  $M$  corresponds to either the longitudinal or the transverse modulus,  $m$  and  $f$  correspond to matrix and fibre respectively,  $V_f$  is the fibre volume fraction and  $\xi$  is the form factor. To calculate the longitudinal modulus  $E_L$  for a longitudinally oriented particle of length  $L$  and diameter  $d$ , the form factor can be given by Equation 5:

$$\xi = \frac{2*L}{d} \quad Eq. 5$$

Where  $L/d$  is the reinforcement material aspect ratio. For the transverse modulus  $E_T$ , satisfactory results have been obtained with  $\xi = 2$  [57].

The modulus of a ply reinforced by randomly dispersed fibres is given by the following expression [57]:

$$E_{mat} = \frac{3}{8}E_L + \frac{5}{8}E_T \quad Eq. 6$$

Where  $E_L$  is the longitudinal modulus and  $E_T$  the transverse modulus of the unidirectional ply (reinforced by unidirectional short fibres), determined from Equations 3 and 4. The assumptions used in these models are a random in-plane fibre distribution, the absence of skin/core distribution effects for estimation purposes, and a homogeneous distribution of particles to understand the reinforcing role of flax shives. Results of this micromechanical model are given in Table 2 and show a good correlation between the measured and estimated stiffness.

The simplified approach used in this study makes it possible to estimate the stiffness of flax shives as reinforcement of injection moulded composites and to explain the reinforcing potential of different types of plant cell walls. Because they are used as short, randomly oriented reinforcement material, their transversal mechanical properties greatly influence the rigidity of the composite. Even if only an estimation, this simplified micromechanical approach allows the study of the impact of the aspect ratio on the mechanical properties of the composite, **which, given its distribution, might explain the differences between the estimated and the measured stiffness.**

To go deeper into this matter, it would be worth taking the skin-core effect into account in addition to the three-dimensional orientation of the reinforcing material, the dispersion in aspect ratio, the elastic properties of the cell walls, and the densification potential of shives during injection. Flax shives are complex natural structures that cannot be considered simply like fibres. Many parameters must be kept in mind, such as variability due to flax variety, growth conditions of the plant, maturity of the stems at pull-out, retting and following mechanical transformation (scutching, grinding, and sieving). Nevertheless, the reinforcing efficiency of flax shives, originating from the xylem, is significant and offers a new field of application to this low added value agricultural by-product.

#### **4. Conclusion**

Flax shives, viewed as a suitable reinforcement material for injection-moulded composite applications, have been investigated from the cell wall scale to that of the stem followed by a mechanical characterisation of injection-moulded composites. The flax xylem is made of both tracheid and vessel elements playing a role in water and sap conduction and the mechanical support of the stem. At the stem level, the distribution of cell surface and cell wall thickness differs on transversal cross-sections and shows a gradient in morphology. The indentation modulus of the xylem cells was investigated by AFM-PFQNM analysis, with stiffness reaching 20-22 GPa and 16 GPa for the S2 and S3 cell wall layers, respectively. The bending properties of the bottom, middle, and top sections of the xylem in the stem are in the same order of magnitude throughout the stem and justify the use of flax shives as reinforcing material without further industrial sorting.

Finally, industrial flax shives were fragmented and sieved before being integrated into a poly-(propylene) matrix containing 4%-wt of modified anhydride PP. Tensile tests showed that the 400-630  $\mu\text{m}$  sieved

fraction does not differ significantly in mechanical properties when compared to the same flax shives that had not undergone a sieving step in their transformation process. The stiffness of flax shives as present in injected composites was back-calculated, and this simple estimation comes to approximately 24% and 54% of the longitudinal and transverse modulus of flax fibres respectively. This study shows a possible alternative application for the present low added value by-product of the flax scutching industry represented by flax shives.

## 5. Acknowledgements

The authors would like to thank the National Association of Research and Technology for funding Lucile Nuez's thesis in partnership with Van Robaeys Frères and the Dupuy de Lôme Research Institute of the Université de Bretagne-Sud (France). Furthermore, authors would like to thank Dr. David Siniscalco and Dr. Camille Goudenhoofft for their valuable contribution on the AFM-PFQNM investigation. We also thank Mrs. Geslin for English post-editing.

## References

- [1] C. Baley and A. Bourmaud, "Average tensile properties of French elementary flax fibers," *Mater. Lett.*, vol. 122, pp. 159–161, 2014.
- [2] F. Bert, "Lin fibre: Culture et transformation," *Arvalis-Institut du Végétal Paris, Fr.*, 2013.
- [3] P. Evon *et al.*, "Production of fiberboards from shives collected after continuous fiber mechanical extraction from oleaginous flax," *J. Nat. Fibers*, vol. 00, no. 00, pp. 1–17, Jan. 2018.
- [4] W. E. Marshall, L. H. Wartelle, and D. E. Akin, "Flax shive as a source of activated carbon for metals remediation," *BioResources*, vol. 2, pp. 82–90, 2007.
- [5] V. Dubois, A. Leblanc, O. Carpentier, G. Alhaik, and E. Wirquin, "Performances of flax shive-based lightweight composites with rapid hardening," *Constr. Build. Mater.*, vol. 165, pp. 17–27, 2018.
- [6] S. González-García, L. Luo, M. T. Moreira, G. Feijoo, and G. Huppes, "Life cycle assessment of flax shives derived second generation ethanol fueled automobiles in Spain," *Renew. Sustain. Energy Rev.*, vol. 13, no. 8, pp. 1922–1933, Oct. 2009.
- [7] A. O. Ogah and J. N. Afiukwa, "Characterization and comparison of mechanical behavior of agro

- fiber-filled high-density polyethylene bio-composites,” *J. Reinf. Plast. Compos.*, vol. 33, no. 1, pp. 37–46, Jan. 2014.
- [8] W. Hu, M. Zhang, M.-T. Ton-That, and T. Ngo, “A comparison of flax shive and extracted flax shive reinforced PP composites,” *Fibers Polym.*, vol. 15, no. 8, pp. 1722–1728, Aug. 2014.
- [9] L. Nuez *et al.*, “The potential of flax shives as reinforcements for injection moulded polypropylene composites,” *Ind. Crop. Prod.*, vol. 148, no. March, p. 112324, 2020.
- [10] K. Ross and G. Mazza, “Characteristics of Lignin from Flax Shives as Affected by Extraction Conditions,” *Int. J. Mol. Sci.*, vol. 11, no. 10, pp. 4035–4050, Oct. 2010.
- [11] A. U. Buranov and G. Mazza, “Extraction and characterization of hemicelluloses from flax shives by different methods,” *Carbohydr. Polym.*, vol. 79, no. 1, pp. 17–25, 2010.
- [12] A. Day *et al.*, “Lignification in the flax stem: Evidence for an unusual lignin in bast fibers,” *Planta*, vol. 222, no. 2, pp. 234–245, 2005.
- [13] C. Mayer-Laigle, N. Blanc, R. Rajaonarivony, and X. Rouau, “Comminution of Dry Lignocellulosic Biomass, a Review: Part I. From Fundamental Mechanisms to Milling Behaviour,” *Bioengineering*, vol. 5, no. 2, p. 41, 2018.
- [14] N. Graupner, J. Rößler, G. Ziegmann, and J. Müssig, “Fibre/matrix adhesion of cellulose fibres in PLA, PP and MAPP: A critical review of pull-out test, microbond test and single fibre fragmentation test results,” *Compos. Part A Appl. Sci. Manuf.*, vol. 63, pp. 133–148, 2014.
- [15] J. Andersons, E. Sparnins, E. Joffe, and L. Wallström, “Strength distribution of elementary flax fibres,” *Compos. Sci. Technol.*, vol. 65, pp. 693–702, 2005.
- [16] K. Charlet, C. Baley, C. Morvan, J. P. Jernot, M. Gomina, and J. Bréard, “Characteristics of Hermès flax fibres as a function of their location in the stem and properties of the derived unidirectional composites,” *Compos. Part A Appl. Sci. Manuf.*, vol. 38, no. 8, pp. 1912–1921, Aug. 2007.
- [17] P. C. Kersavage, “A system for automatically recording the load-elongation characteristics of single wood fibers under controlled relative humidity conditions.,” 1973.
- [18] M. Eder, S. Stanzl-tschegg, and I. Burgert, “The fracture behaviour of single wood fibres is governed by geometrical constraints : in situ ESEM studies on three fibre types,” *Wood Sci. Technol.*, vol. 42, pp. 679–689, 2008.

- [19] W. Gindl, H. S. Gupta, T. Schöberl, H. C. Lichtenegger, and P. Fratzl, “Mechanical properties of spruce wood cell walls by nanoindentation,” *Appl. Phys. A*, vol. 79, no. 8, pp. 2069–2073, Dec. 2004.
- [20] O. Arnould, D. Siniscalco, A. Bourmaud, A. Le Duigou, and C. Baley, “Better insight into the nano-mechanical properties of flax fibre cell walls,” *Ind. Crops Prod.*, vol. 97, pp. 224–228, Mar. 2017.
- [21] A. Bourmaud and C. Baley, “Nanoindentation contribution to mechanical characterization of vegetal fibers,” *Compos. Part B Eng.*, vol. 43, no. 7, pp. 2861–2866, 2012.
- [22] P. Perre, A. T. Dinh, C. Assor, X. Frank, and G. Pilate, “Stiffness of normal, opposite, and tension poplar wood determined using micro-samples in the three material directions,” *Wood Sci. Technol.*, vol. 47, no. 3, pp. 481–498, May 2013.
- [23] D. U. Shah, T. P. S. Reynolds, and M. H. Ramage, “The strength of plants: Theory and experimental methods to measure the mechanical properties of stems,” *J. Exp. Bot.*, vol. 68, no. 16, pp. 4497–4516, 2017.
- [24] S. Réquillé, C. Goudenhoft, A. Bourmaud, A. Le Duigou, and C. Baley, “Exploring the link between flexural behaviour of hemp and flax stems and fibre stiffness,” *Ind. Crops Prod.*, vol. 113, no. January, pp. 179–186, 2018.
- [25] H. S. S. Sharma, G. Faughey, and G. Lyons, “Comparison of physical, chemical, and thermal characteristics of water-, dew-, and enzyme-retted flax fibers,” *J. Appl. Polym. Sci.*, vol. 74, no. 1, pp. 139–143, 2002.
- [26] A. Lefeuvre, A. Bourmaud, L. Lebrun, C. Morvan, and C. Baley, “A study of the yearly reproducibility of flax fiber tensile properties,” *Ind. Crops Prod.*, vol. 50, pp. 400–407, 2013.
- [27] G. Coroller, “Contribution à l’étude des matériaux composites renforcés par des fibres végétales: cas des composites extrudés à matrice polypropylène,” Lorient, 2013.
- [28] C. Goudenhoft *et al.*, “Investigation of the mechanical properties of flax cell walls during plant development: The relation between performance and cell wall structure,” *Fibers*, vol. 6, no. 1, 2018.
- [29] C. M. Popescu, G. Singurel, M. C. Popescu, C. Vasile, D. S. Argyropoulos, and S. Willför, “Vibrational spectroscopy and X-ray diffraction methods to establish the differences between

- hardwood and softwood,” *Carbohydr. Polym.*, vol. 77, no. 4, pp. 851–857, 2009.
- [30] E. L. Taylor, T. N. Taylor, and M. Krings, “Introduction to Vascular Plant Morphology and Anatomy,” in *Paleobotany: the biology and evolution of fossil plants*, Academic Press, 2009, pp. 201–222.
- [31] P. Barlow, *From Cambium to Early Cell Differentiation Within the*. Elsevier Inc., 2005.
- [32] K. Nieminen, T. Blomster, Y. Helariutta, and A. P. Mähönen, “Vascular Cambium Development,” *Arab. B.*, vol. 13, p. e0177, 2015.
- [33] C. Lion *et al.*, “BLISS: A Bioorthogonal Dual-Labeling Strategy to Unravel Lignification Dynamics in Plants,” *Cell Chem. Biol.*, vol. 24, no. 3, pp. 326–338, 2017.
- [34] A. Day *et al.*, “Caffeoyl coenzyme A O-methyltransferase down-regulation is associated with modifications in lignin and cell-wall architecture in flax secondary xylem,” *Plant Physiol. Biochem.*, vol. 47, no. 1, pp. 9–19, Jan. 2009.
- [35] E. Fernandez-Tendero, A. Day, S. Legros, A. Habrant, S. Hawkins, and B. Chabbert, “Changes in hemp secondary fiber production related to technical fiber variability revealed by light microscopy and attenuated total reflectance Fourier transform infrared spectroscopy,” *PLoS One*, vol. 12, no. 6, pp. 1–14, 2017.
- [36] F. Sterky *et al.*, “Gene discovery in the wood-forming tissues of poplar: Analysis of 5,692 expressed sequence tags,” *Proc. Natl. Acad. Sci. U. S. A.*, vol. 95, no. 22, pp. 13330–13335, 1998.
- [37] A. J. Panshin and C. de Zeeuw, “Textbook of wood technology. Volume I. Structure, identification, uses, and properties of the commercial woods of the United States and Canada.,” *Textb. wood Technol. Vol. I. Struct. identification, uses, Prop. Commer. woods United States Canada.*, no. 3rd ed., 1970.
- [38] A. M. Patten, D. G. Vassão, M. P. Wolcott, L. B. Davin, and N. G. Lewis, “Trees: A remarkable biochemical bounty,” *Compr. Nat. Prod. II Chem. Biol.*, vol. 3, pp. 1173–1296, 2010.
- [39] S. Carlquist and E. L. Schneider, “The tracheid-vessel element transition in angiosperms involves multiple independent features: Cladistic consequences,” *Am. J. Bot.*, vol. 89, no. 2, pp. 185–195, 2002.
- [40] J. S. Sperry, “Evolution of water transport and xylem structure,” *Int. J. Plant Sci.*, vol. 164, no. SUPPL. 3, 2003.

- [41] N. Tiver, “Studies of the flax plant Part 1 Physiology of growth, stem anatomy and fibre development in fibre flax,” *Aust. J. Exp. Biol. Med. Sci.*, vol. 20, no. 3, pp. 149–160, Sep. 1942.
- [42] A. Lefeuvre, A. Bourmaud, and C. Baley, “Optimization of the mechanical performance of UD flax/epoxy composites by selection of fibres along the stem,” *Compos. Part A Appl. Sci. Manuf.*, vol. 77, pp. 204–208, Oct. 2015.
- [43] J. Beaugrand, M. Nottez, J. Konnerth, and A. Bourmaud, “Multi-scale analysis of the structure and mechanical performance of woody hemp core and the dependence on the sampling location,” *Ind. Crops Prod.*, vol. 60, pp. 193–204, 2014.
- [44] A. Melelli, O. Arnould, J. Beaugrand, and A. Bourmaud, “The Middle Lamella of Plant Fibers Used as Composite Reinforcement: Investigation by Atomic Force Microscopy,” *Molecules*, vol. 25, no. 3, p. 632, Feb. 2020.
- [45] A. Bourmaud *et al.*, “Evolution of flax cell wall ultrastructure and mechanical properties during the retting step,” *Carbohydr. Polym.*, vol. 206, no. May 2018, pp. 48–56, 2019.
- [46] P. Mikshina, T. Chernova, S. Chemikosova, N. Ibragimova, N. Mokshina, and T. Gorshkova, “Cellulosic Fibers: Role of Matrix Polysaccharides in Structure and Function,” in *Cellulose - Fundamental Aspects*, InTech, 2013, pp. 91–112.
- [47] A. Jäger, T. Bader, K. Hofstetter, and J. Eberhardsteiner, “The relation between indentation modulus , microfibril angle , and elastic properties of wood cell walls,” *Compos. - Part A Appl. Sci. Manuf.*, vol. 42, pp. 677–685, 2011.
- [48] K. Schulgasser and A. Witztum, “On the strength, stiffness and stability of tubular plant stems and leaves,” *J. Theor. Biol.*, vol. 155, no. 4, pp. 497–515, 1992.
- [49] G. Değer *et al.*, “Strength of Wheat and Barley Stems and Design of New Beam/Columns,” *Math. Comput. Appl.*, vol. 15, no. 1, pp. 1–13, Apr. 2010.
- [50] N. Wang, W. Liu, J. Huang, and K. Ma, “The structure-mechanical relationship of palm vascular tissue,” *J. Mech. Behav. Biomed. Mater.*, vol. 36, pp. 1–11, 2014.
- [51] Ö. P. Çetinkol *et al.*, “Structural and Chemical Characterization of Hardwood from Tree Species with Applications as Bioenergy Feedstocks,” *PLoS One*, vol. 7, no. 12, p. e52820, Dec. 2012.
- [52] L. J. Gibson, “The hierarchical structure and mechanics of plant materials,” *J. R. Soc. Interface*, vol. 9, no. 76, pp. 2749–2766, Nov. 2012.

- [53] M.-C. Trouy-Triboulot and P. Triboulot, “Matériau bois Structure et caractéristiques,” *Tech. l’Ingénieur*, vol. 33, no. 0, pp. 0–26, 2001.
- [54] M. Le Gall, P. Davies, N. Martin, and C. Baley, “Recommended flax fibre density values for composite property predictions,” *Ind. Crops Prod.*, vol. 114, no. February, pp. 52–58, 2018.
- [55] A. Amiri, Z. Triplett, A. Moreira, N. Brezinka, M. Alcock, and C. A. Ulven, “Standard density measurement method development for flax fiber,” *Ind. Crop. Prod.*, vol. 96, pp. 196–202, 2017.
- [56] J. C. Halpin and J. L. Kardos, “The Halpin-Tsai Equations: A Review,” *Polym. Eng. Sci.*, vol. 16, no. 5, pp. 344–352, 1976.
- [57] R. F. Gibson, *Principles of Composite Material Mechanics*. 1994.
- [58] C. Baley, Y. Perrot, F. Busnel, H. Guezenoc, and P. Davies, “Transverse tensile behaviour of unidirectional plies reinforced with flax fibres,” *Mater. Lett.*, vol. 60, no. 24, pp. 2984–2987, 2006.
- [59] C. Baley, M. Gomina, J. Breard, A. Bourmaud, and P. Davies, “Variability of mechanical properties of flax fibres for composite reinforcement. A review,” *Ind. Crops Prod.*, vol. 145, no. September, p. 111984, 2020.
- [60] C. Baley, A. Kervoëlen, A. Le Duigou, C. Goudenhoft, and A. Bourmaud, “Is the low shear modulus of flax fibres an advantage for polymer reinforcement?,” *Mater. Lett.*, vol. 185, pp. 534–536, 2016.
- [61] D. D. Scida, A. Bourmaud, and C. Baley, “Influence of the scattering of flax fibres properties on flax/epoxy woven ply stiffness,” *Mater. Des.*, vol. 122, pp. 136–145, 2017.
- [62] Forest Products Laboratory, “Wood Handbook-Wood as an Engineering Material,” 2010.

### Figure captions

**Figure 1.** a. Xylem sample preparation along the length of the stem with C0 to C4 as the five regions of interest. Grey arrows represent the vibratome slicing locations. Inspired from [28]. b. SEM image of the flax stem cross-section, showing the presence of bast fibres (bf) surrounding the xylem tissue (xyl).

**Figure 2.** SEM observations of sieved flax shive fraction (400 - 630  $\mu\text{m}$ ).

**Figure 3.** Flax stem tissue organization: a. computer reconstituted picture after X ray nanotomography; b-e. SEM images from flax stem cross-sections; c and e are magnifications of b and d photographs respectively. At: Annular tracheid, Bf: Bast fibres, Cp: Cortical Parenchyma, Ep: Epidermis, Ft: Fibre tracheid, Ht: Helicoidal tracheid, Pcw: Primary cell wall, Ph: Pith, Pt: pit, P xyl: Primary xylem, S xyl: Secondary xylem, Rp: Ray parenchyma, Scw: Secondary cell wall, Sv: Scalariform tracheid, Td: Tracheid, Vc: Vascular cambium, Vs: Vessel.

**Figure 4.** Evolution of the xylem and pith surface and xylem tissue thickness with sampling location, with SEM observations at the different sampling locations. The positions of each location are clearly specified in Figure 1.

**Figure 5.** a, b, c. Surface distribution cells in the xylem tissue as a function of stem height (a for C1, b. for C2 and c. for C3), d, e, f. Evolution of the mean cell surface as a function of their normalised position in the xylem tissue for C1, C2, and C3 respectively.

**Figure 6.** Cell wall thickness distribution in the xylem tissues as a function of stem height for a. C1, b. C2, c. C3.

**Figure 7.** a. AFM PF-QNM mapping of the indentation modulus of the flax xylem taken at fibre maturity stage, the dotted area indicates the region deeply explored in subfigure b. Focus with indication of xylem cell wall sub-layers: ML: middle lamella, P: primary cell wall, S1, S2 and S3: first, second and third layer of the secondary cell wall. c. Evolution of the indentation modulus according to the white line in subfigures a. and b.

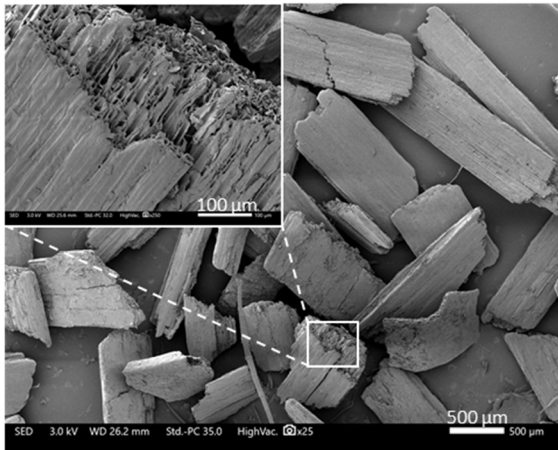
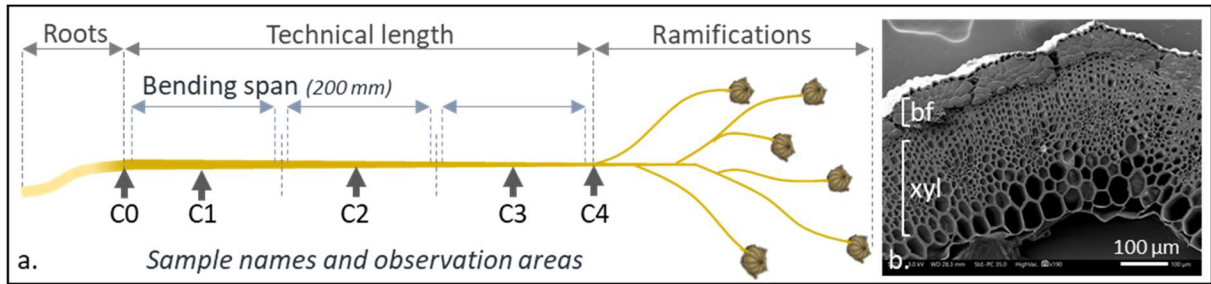
### **Table captions**

**Table 1.** Apparent modulus of the xylem as a function of its location in the stem as a result of 3-point bending tests.

**Table 2.** Experimental and estimated injection-moulded stiffness as a function of mass fraction and mean aspect ratio of a panel of reinforcing materials. The data of samples with \* are taken from our previous study [9]. PP, FS, FF and WF refer to poly-(propylene), flax shives, flax fibres and wood flour respectively.

**Table 3.** Density, longitudinal and transversal modulus of flax fibres, softwood, and flax shives.

Colour should be used for all figures in the manuscript.



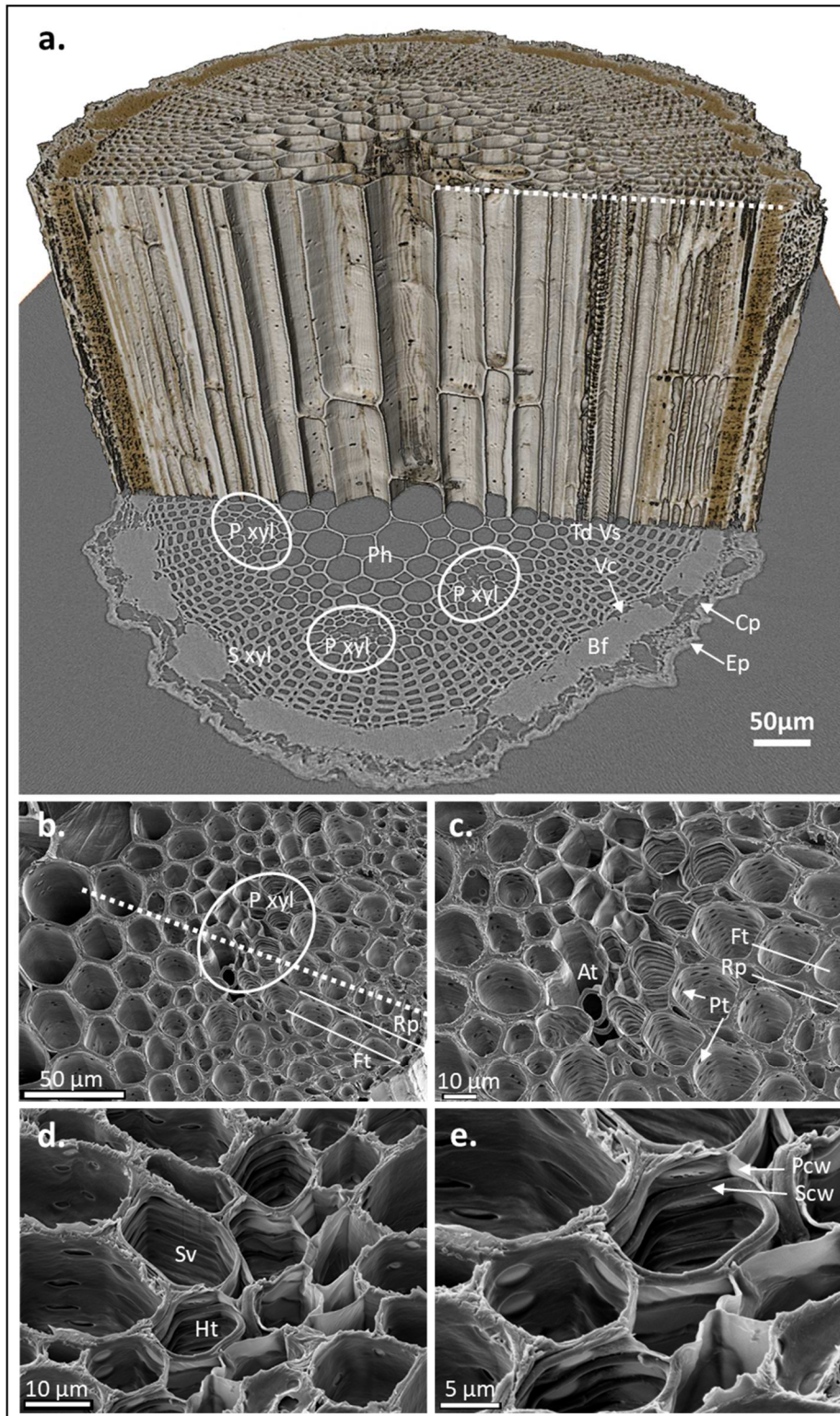


Figure 3. Flax stem tissue organization: a. computer reconstituted picture after X ray nanotomography; b-e. SEM images from flax stem cross-sections; c and e are magnifications of b and d photographs respectively. At: Annular tracheid, Bf: Bast fibres, Cp: Cortical Parenchyma, Ep: Epidermis, Ft: Fibre tracheid, Ht: Helicoidal tracheid, Pcw: Primary cell wall, Ph: Pith, Pt: pit, P xyl: Primary xylem, S xyl: Secondary xylem, Rp: Ray parenchyma, Scw: Secondary cell wall, Sv: Scalariform tracheid, Td: Tracheid, Vc: Vascular cambium, Vs: Vessel.

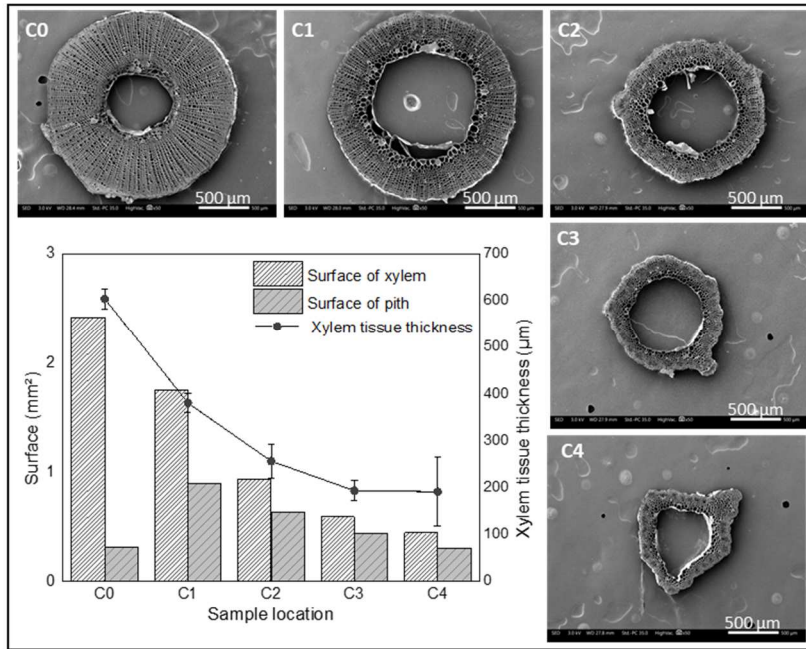


Figure 4. Evolution of the xylem and pith surface and xylem tissue thickness with sampling location, with SEM observations at the different sampling locations. The positions of each location are clearly specified in Figure 1.

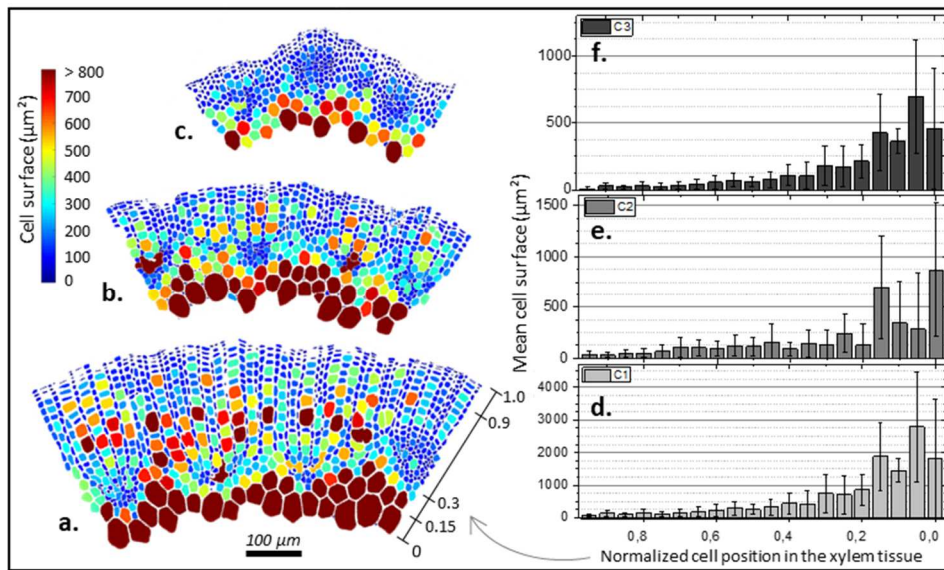


Figure 5. a, b, c. Surface distribution cells in the xylem tissue as a function of stem height (a for C1, b. for C2 and c. for C3), d, e, f. Evolution of the mean cell surface as a function of their normalised position in the xylem tissue for C1, C2, and C3 respectively.

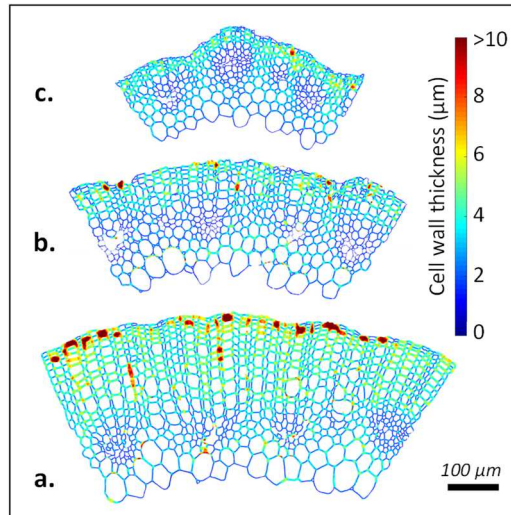


Figure 6. Cell wall thickness distribution in the xylem tissues as a function of stem height for a. C1, b. C2, c. C3.

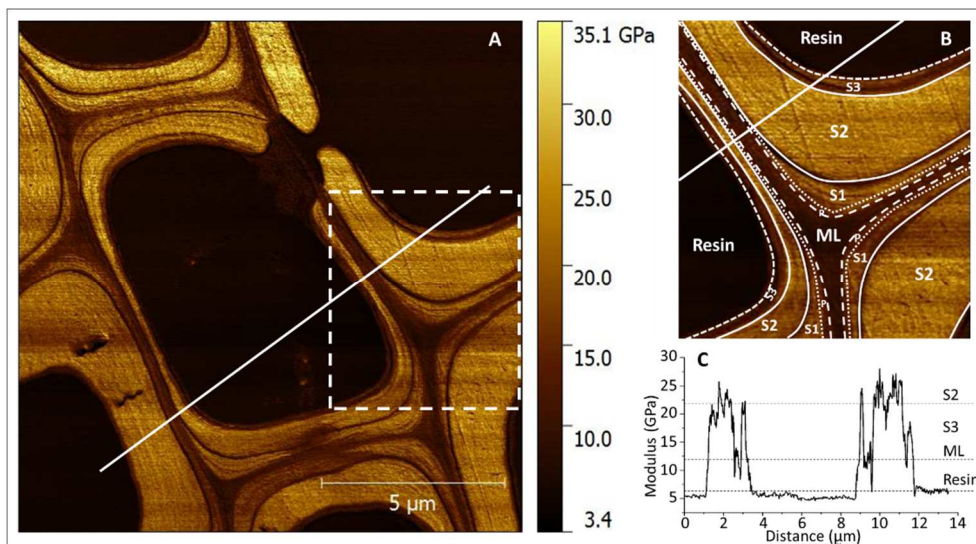


Figure 7. a. AFM PF-QNM mapping of the indentation modulus of the flax xylem taken at fibre maturity stage, the dotted area indicates the region deeply explored in subfigure b. Focus with indication of xylem cell wall sub-layers: ML: middle lamella, P: primary cell wall, S1, S2 and S3: first, second and third layer of the secondary cell wall. c. Evolution of the indentation modulus according to the white line in subfigures a. and b.

Table 1. Apparent modulus of the xylem as a function of its location in the stem as a result of 3-point bending tests.

Sample location in the stem	Apparent modulus (MPa)	
	Mean	S. D.
C1 - Bottom	6,223	710
C2 - Middle	6,160	597
C3 - Top	7,123	781

Table 2. Experimental and estimated injection-moulded stiffness as a function of mass fraction and mean aspect ratio of a panel of reinforcing materials. The data of samples with \* are taken from our previous study [9]. PP, FS, FF and WF refer to poly-(propylene), flax shives, flax fibres and wood flour respectively.

Samples	PP	PP + FS (sieved 400- 630 $\mu\text{m}$ )	PP + FS (500 $\mu\text{m}$ milling grid)	PP + FS (250 $\mu\text{m}$ milling grid)	PP + FS (attrition milling 50 $\mu\text{m}$ )	PP + FF & FS (1 mm and 500 $\mu\text{m}$ milling grid)	PP + FF (1 mm)	PP + WF ( $< 800 \mu\text{m}$ )
<i>Measured tensile properties</i>								
<b>E<sub>exp</sub> (MPa)</b>	1,545 $\pm 73$	3,176 $\pm 464$	3,268 $\pm 239^*$	2,815 $\pm 86^*$	2,269 $\pm 185^*$	3,302 $\pm 83^*$	3,668 $\pm 90^*$	2,907 $\pm 73^*$
<b>M<sub>f</sub> (%)</b>	-	30	30	30	30	30	30	30
<b>Density (g/cm<sup>3</sup>)</b>	0.91	-	1	1.01	1.01	1.01	1.02	1.01
<b>V<sub>f</sub> (%)</b>	-	24	24	24	24	22	20	46
<b>Mean L/D</b>	-	5.1 $\pm$ 1.6	4.8 $\pm$ 2.4*	3.7 $\pm$ 2.1*	2.7 $\pm$ 1.6*	7.5 $\pm$ 5.3*	11 $\pm$ 6.2*	5.1 $\pm$ 2.9*
<i>Estimated tensile tangent modulus</i>								
<b>E<sub>est</sub> (MPa)</b>	-	2,724	2,694	2,571	2,502	3,403	3,703	2,780
<b>Difference (%)</b>	-	-14.2	-17.6	-8.7	10.3	3.1	1.0	-4.4

Table 3. Density, longitudinal and transversal modulus of flax fibres, softwood, and flax shives.

	Density (g/cm <sup>3</sup> )	Longitudinal modulus (MPa)	Transversal modulus (MPa)	Ref.
<b>Flax fibres</b>	1.5	52,300	8,000	[54], [58]–[61]
<b>Softwood</b>	0.45	13,100	818	[53] [62]
<b>Flax shives</b>	1.237	27,930	3,280	Estimate: this work